Hydrogen fuel cell scooter with plug-out features for combined transport and residential power generation

Robledo, Carla; van Leeuwen, Lotta; van Wijk, Ad

DOI
10.1016/j.ijhydene.2019.04.103

Publication date
2019

Document Version
Final published version

Published in
International Journal of Hydrogen Energy

INTERNATIONAL JOURNAL OF HYDROGEN ENERGY 44 (2019) 29648–29657

Available online at www.sciencedirect.com

ScienceDirect

journal homepage: www.elsevier.com/locate/he

Hydrogen fuel cell scooter with plug-out features for combined transport and residential power generation

Carla B. Robledo[*], *Lotta B. van Leeuwen*, *Ad J.M. van Wijk*

Energy Technology Section, Department of Process and Energy, Delft University of Technology, Leeghwaterstraat 39, 2628 CB Delft, the Netherlands

ARTICLE INFO

Article history:
Received 19 December 2018
Received in revised form
19 March 2019
Accepted 10 April 2019
Available online 9 May 2019

Keywords:
V2G
V2L
Electric mobility
Hydrogen
Power generation

ABSTRACT

The need for zero emission drive is a global necessity that can contribute to mitigate greenhouse gas emissions. In this context, fuel cell hybrid electric vehicles are increasingly attracting interest by governments, companies and academia. While parked they can operate as power generation units, given the proper connection to the electricity grid via vehicle-to-grid integration (V2G), or even power appliances directly (Vehicle-to-Load, V2L). In this study, we analysed the use of a hydrogen fuel cell electric scooter in combined driving, V2G and V2L mode. V2G resulted in the most efficient mode of the three, while V2L led to higher degradation rates. The measured average cell voltage degradation rate was 209 μV/h for driving mode, 356 μV/h for V2G and 648 μV/h for V2L. The insights provided in this study are useful to develop new, optimized and specifically targeted energy management systems for power generation of hydrogen hybrid electric drive vehicles.

Introduction

The urgency to reduce anthropogenic impact on climate is felt around the globe. Despite the large international efforts to reduce CO_2 emissions, in 2017 global energy-related CO_2 emissions grew by 1.4% [1]. In view of these results, the energy system needs to be fully transformed from fossil to renewables. In the electricity sector, wind turbines and photovoltaics are overtaking the renewable energy market rapidly [2]. As well, conventional, centralized power plants are making room for more distributed energy production [3]. This intermittent power generation of these technologies brings about new challenges when it comes to flexibility of supply. The trend in the transport sector is electrification of power trains, either fuelled by batteries or fuel cells. The reason to replace internal combustion engines is not only because of the CO_2 emissions but also volatile compounds and particulate matter, which are of great threat to the environment and human health. It has been recently reported that, particularly scooters, can dominate urban vehicular pollution above cars and trucks [4].

Integration of electricity and transport systems into a single energy system is a possibility to offer greater flexibility while increasing utilization, efficiency and reducing overall costs [5]. A smart grid is a local unit of such an integrated energy system. The energy is produced, transformed and consumed locally. Flexibility is created by physical storage

* *Corresponding author.*
E-mail address: c.b.robledo@minezk.nl (C.B. Robledo).
https://doi.org/10.1016/j.ijhydene.2019.04.103

instruments as well as market instruments, such as electrical storage units, conversion to fuel, controllers, price indexing. These components must balance the micro-level generation and consumption together with the macro-level interconnections [6]. Taking this concept one step further, the transport system can also be integrated into this smart energy system. Vehicles are often parked close to buildings and are most of the time not in use [7]. Designing and managing vehicles to be part of buildings makes them a potential tool for environmental and economic savings. Recent studies consider electric vehicles as active components of the building's energy systems, including bidirectional energy exchange with the house and grid, solar PV roof top production, and energy storage systems [8,9]. Results vary, but depending on the scenarios and assumptions made, electricity consumption in these buildings is usually reduced from 30 to 70% by this integration approach [10,11].

Worldwide urbanization is asking for more lightweight vehicles, which are easy to park and offer enough flexibility for daily commuting. Two-wheelers have been taking over the urban landscape in developing countries. Two-stroke scooters are popular globally, particularly in Asia, Africa and Southern Europe, with a global annual production of more than 25 million vehicles [4,12]. Up to 95% of the motor vehicles on road in Asia are motorcycles [13]. Therefore, the development of zero-emission scooters is important to improve air quality and protect the environment. As well, the concept of a "green hydrogen economy", where hydrogen is the carbon-free energy carrier and fuel is gaining momentum [14]. Both the Japanese and the German government are investing in hydrogen fuelling infrastructure to meet up the vehicle-fleet development [15–17]. The cost of sustainable hydrogen production is the limiting factor now, which might be overcome in a near future [18,19]. All these aspects combined, have led to several investigations and development of fuel cell powered scooters. Since fuel cells are characterized by slow dynamics, fuel cell scooters are usually of hybrid nature [20]; In this way, the power system architecture is composed of the main power system, a fuel cell stack, and a secondary energy source, usually a battery or supercapacitor. The preferred fuel cell technology for these scooters is the Proton Exchange Membrane (PEM) fuel cell, since they pose the benefits of rapid start-up, low operating temperatures, and high power densities. The secondary energy source is used to enhance the scooter driving range, improve the performance at cold starts, and reduce overall system costs [21]. State-of-the art power system architecture combine PEM FC with lithium batteries [22]. The main advantage of using a battery over supercapacitor is that they provide a larger storage capacity. Asian Pacific Fuel Cell Technologies (APFCT) company has designed a hydrogen scooter based on a PEM FC stack and a lithium-NMC battery, which the Taiwanese government has implemented in a trial promoting the use of zero-emission scooters [23].

As the penetration of fuel cell electric vehicles (FCEVs) on the market is increasing, the question of integrating these vehicles into the energy system and the built environment, through vehicle-to-grid (V2G) technology for example, arises. In 1997, Kempton et al. already proposed the idea that electric vehicles, either propelled by hydrogen via a fuel cell or electrochemical energy stored in batteries, would have value to electricity utilities as power resources [24]. They furthered analysed the economic potential of the integration of such vehicles into the electricity system via V2G [25]. There have been recent techno-economic analysis on the feasibility of integrating single buildings, communities and smart cities with hydrogen FCEVs operating in V2G [26,27]. Nonetheless, little is known on the main technical difficulties with respect to fuel cell degradation and reliability of FCEVs operating in V2G. In our previous studies we have demonstrated the connection of a fuel cell electric car to the Dutch electrical grid providing V2G services [28]. As well the connection of a residential building operating in V2G mode was studied. And we have analysed the possibility of providing vehicle-to-load (V2L) services, in which the electricity is fed directly to appliances [29]. Such usage can aid in reducing the residential grid electricity consumption and can help stabilize the grid during peak demand. Inspired by these findings, in this paper we aim to evaluate the use of a fuel cell electric scooter (FCES) also operating in V2G and V2L modes.

To get insights about this topic, an experimental study was performed using a FCES manufactured by APFCT. The scooter's power source is hybrid: the fuel cell is connected to a battery accounting for the peak power demand and a DC/DC converter to meet the energy distribution control requirements [30]. Therefore, the performance of the FCES is dependent on the performance of the fuel cell, but also on the battery and converter. As it has been pointed out in a recent review article, in order to analyse such hybrid and complex systems, system-level research on durability against the actual automotive application are urgently needed [31]. For such purpose, the scooter was tested in three modes: to drive, to provide power to appliances (V2L) and to provide power to the grid (V2G). In this study, the combined use of the scooter for driving and power generation and its effect on the overall system performance is explored. The main original aspects of this work are:

- First time performance analysis of a hydrogen scooter operating in combined driving and vehicle-to-electricity modes.
- Implementation of multivariate statistical analysis for degradation analysis of fuel cell in combined V2G, V2L and driving mode.
- Identification of the most degrading mode, of the three ones tested.
- Suggestion for improved energy management systems for vehicle-to-electricity modes, different to that one for driving (in order to minimize fuel cell degradation).

Materials and methods

Characteristics of hydrogen fuel cell scooter

The scooter used for this study is a FCES model 4.8 from APFCT, shown in Fig. 1a. The scooter's power system is illustrated in Fig. 1b and is essentially composed of a Proton Exchange Membrane (PEM) fuel cell stack (FC), an air blower, a

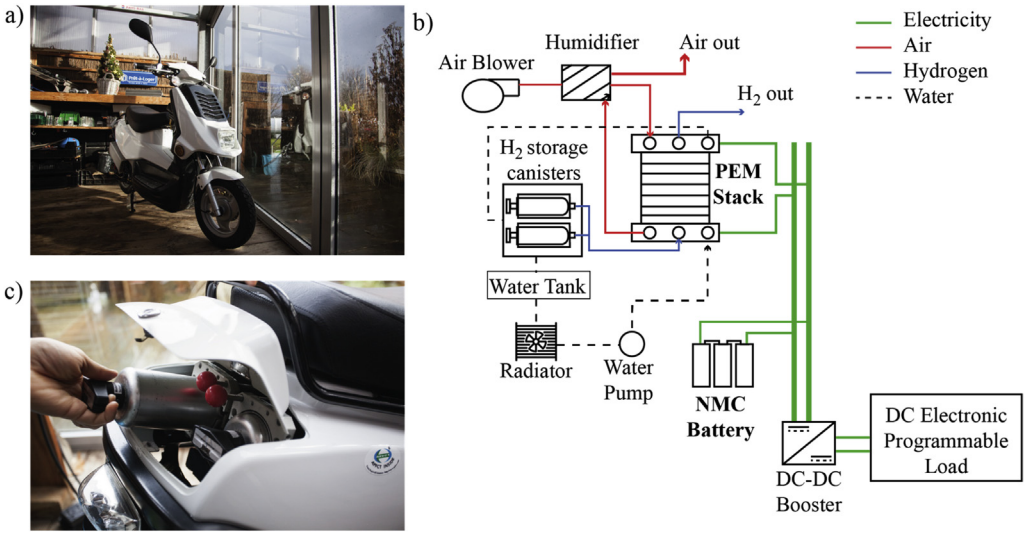

Fig. 1 – a) APFCT hydrogen electric scooter model 4.8. b) Schematic drawing of the scooter hybrid power system (with the connection to the programmable load for experiments) and balance of plant components of the fuel cell system. c) Picture of the hydrogen storage canisters in the rear part of the scooter.

water pump, a Lithium Nickel Manganese Cobalt Oxide (Li-NMC) battery, a DC-DC converter and hydrogen storage canisters (HSC). It is an improved version of model 4.5, which had a smaller FC and an ultracapacitor as well. Detailed systems configuration and control of this previous model (which mostly still applies to version 4.8) can be found in this reference [32]. The schematics show the scooter connected to a programmable load that is used in the experiments to simulate the driving, vehicle-to-grid and vehicle-to-load patterns. Table 1 presents the specifications of the main components of the scooter.

The fuel cell is the main power supplier, while the battery accounts for peaking power demand. The fuel cell stack and the battery are placed in parallel, which means all combinations are possible to power the loads: only FC, only battery or both FC and battery. The battery is only charged via the FC, there is no plug for external electric charging. The DC/DC booster then transforms 24 V from the power sources to 48 VDC, which is needed by the power sink components (motor, grid, electrical appliances).

All the components supporting the fuel cell stack compose the Balance of Plant (BoP). These include the blower, which feeds air into the system; the humidifier, which is necessary to allow proton transfer through the membrane and to control water flooding of the cathode; the water pump, which keeps water flow at the correct rate; and a stack coolant system (water, black dashed line in Fig. 1b), which prevents excessive temperature rise of the fuel cell stack. This is done by extracting the waste heat from the fuel cell stack and reutilise it to desorb hydrogen by circulating it through an external water jacket around the HSC. The process of hydrogen desorption in metal hydrides is endothermic. So by utilising the waste heat from the fuel cell the system's overall efficiency is increased.

The only external energy input of the scooter is the hydrogen, which is stored in metal hydrides in two low-pressure alloy canisters in the rear part of the scooter, as is shown in Fig. 1c. The two canisters are contained in the scooter in easy plug-in/plug-out holders. The maximum amount of available hydrogen contained in both canisters is 90 g, which allows a driving range of approximately 50 km. In this study, hydrogen is charged via a self-made lab hydrogen supply connection from 200 bar bottles, as shown in the scheme on Fig. 2.

The hydrogen pressure is further reduced to 10 bar to charge the metal hydride canisters. While charging, the canisters are submerged in a temperature controlled water bath to avoid raise of temperature of the canisters, due to the exothermic hydrogen absorption process. It takes approximately 40 min to charge both canisters at the same time completely.

Table 1 – Specifications of fuel cell, battery hydrogen canisters and DC/DC booster in the scooter.

Component	Item	Value
PEM Fuel Cell	Rated power	2400 W
	Rated voltage	24 V
	Operating voltage	21–33 V
	Max. power in V2G & V2L	1200 W
	Rated current	100 A
	Nr. of cells	40
Li-NMC Battery	Nominal voltage	24 V
	Rated capacity	20 Ah
Hydrogen Canister	Material of metal hydride	AB5 alloy
	Hydrogen stored per canister	45 g
	Number of canisters	2
DC/DC Booster	Output Voltage	48 VDC
	Rated input voltage	24 VDC
	Input voltage range	22-40 VDC
	Max. power	2500 W
	Operating efficiency	96%
	Max. input current	125 A

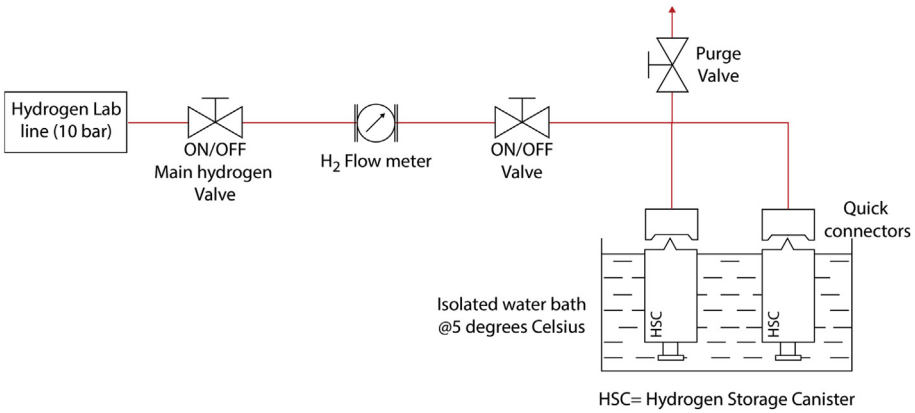

Fig. 2 – Scheme of the metal hydride canisters charging station implemented at the laboratory at Delft University of Technology.

Experiment

The scooter was previously driven 3122 km in Taiwan before performing the experiments at the lab. Data on this usage was not measured and thus the previous history of the fuel cell and other components is not known. The use of the scooter in three different modes (drive, V2G and V2L) was tested by simulating three patterns in a Kikusui PLZ4-1000W DC electronic programmable load. The load was connected to the DC bus of the scooter and when the load was turned on, the scooter began to supply the demanded power. The scooter was submitted to 30 repetitions per mode, making 90 in total. The order in which the repetitions were performed was determined randomly. Each run lasted 1024 s. Between each run, the scooter was turned off to cool down the system. The 90 repetitions were performed consecutive over a period of 3 months.

In order to collect data under scooter operation, sensors were installed to measure the current and voltage of fuel cell, battery and the output delivered to the load, hydrogen content in the storage system and temperature of the fuel cell, while the runs were performed. Data from each run was stored in Hioki LR8431 logger with a frequency of 1 Hz.

Power demand patterns for the three operating modes

Different power demand patterns were designed to resemble actual driving, vehicle-to-grid and vehicle-to-electrical appliances load patterns. The final implemented power profiles for the three modes are shown in Fig. 3.

The pattern for V2L was designed based on instantaneous power measurements of daily used appliances with a Voltcraft Energy Logger 4000 measuring device. The power consumption signals of 2 charging phones, 2 laptops and one television were added to yield the total profile. The driving cycle applied to the FCES in this study was based on the Taipei Motorcycle Driving Cycle (TMDC), which has been developed with real-data use [33]. It is much closer to real-life driving than a theoretical driving cycle such as the ECE-40 for example. However, since the electronic load used for the experiment can maximum apply 1 kW, some modifications were made to the original TMDC. First, the driving cycle was translated from velocity to instantaneous power demand using the physical model described in Lin's work [34]. Second, the maximum power demand to drive the scooter was truncated from 1.6 kW to 1 kW. Third, a representative segment of the drive cycle was chosen and repeated to match the number of entries of the e-load program. In this way, the main characteristics such as

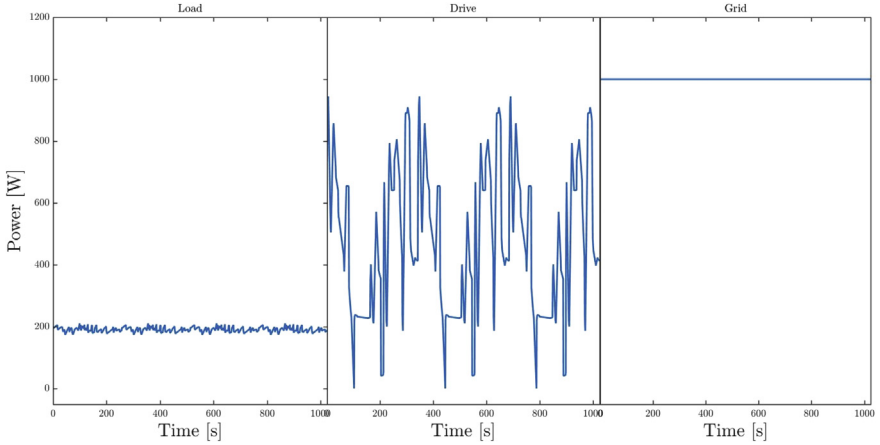

Fig. 3 – Power demand patterns for the three scooter's operation modes tested. From left to right: V2L, Drive and V2G.

high average acceleration and deceleration, low average speed and changing speed were maintained. To mimic the use of the scooter for V2G application, a constant power demand of 1 kW was programmed. This is the maximum power demand possible in this setup, given the size of the DC load. It is close to the scooter's maximum V2G capability of 1.2 kW.

Data analysis

The experiment resulted in 92160 data entries for each variable measured (result from 1024 measurements per run and 30 repetitions per mode). First a descriptive statistical analysis was performed on all the variables measured to understand the distribution of the data under each mode. Then, average values of each variable and for each repetition were obtained and principal component analysis (PCA) was performed on this new data set. PCA is a multivariate technique that constructs new not correlated variables (components), which are linear combination of the original variables, as to maximize the variation between repetitions. These new variables allow studying by parts the variability existent in the data set and permit a different interpretation that many times is not possible from direct observation of the data set [35]. In doing so, we intend to determine whether there are differences in the three modes of operations and which are the variables most responsible of those differences. This technique has been implemented before in the analysis of PEM fuel cell performance under extremely controlled conditions in the lab [36]. They concluded that PCA allows classifying groups of variables, which mostly contribute to stack behaviour. In this study, we aim to extend the analysis to all variables measured in the hybrid electric system present in the scooter. Lastly, an empirical model is deduced using linear regression analysis to determine which mode of operation leads to higher degradation of the fuel cell. Data analyses were done in InfoStat statistical software [37].

Results and discussion

Operation of the hybrid power system in the different modes

Fig. 4 shows the dynamics of the battery and fuel cell in the scooter operating under the three different modes tested. These power values are the average of the 30 repetitions for each mode. In the V2L mode, the battery was rarely used. The total power delivered was lower than the fuel cell limiting-power point of 600 W, and thus it was the only power supplier. The battery was not necessary in V2L, for this specific power demand, and was either charging (Pbatt<0) or in standby (Pbatt = 0). In driving mode, both battery and fuel cell delivered power to fulfil the required demand. The battery was used when a power value higher than 600 W was demanded. Below this point, the fuel cell charged the battery, indicated in Fig. 4 by negative battery power values. In the V2G mode, both fuel cell and battery were needed to supply this power demand, in varying shares along the full experiment. The fuel cell handled the largest part of this demand, with an increasing share from 650 W in the beginning up to 1 kW at the end. The battery provided 550 W at the start, and slowly decreased until it reached the lower limit state of charge, time at which the fuel cell charged it again.

Fig. 4 shows the average behaviour of the modes; while in Fig. 5 the distribution of the variables are presented partitioned by mode.

With respect to the fuel cell, the V2G mode was characterized by higher current values on average than in any other mode, and presented lower voltage values (Fig. 5a and b, respectively). Nonetheless, the drive mode presented a wider range of fuel cell current operation values and the V2L mode a more variable fuel cell voltage (varying from 28 to 31.5 V). Temperature of the fuel cell was on average higher in V2G mode and the lowest in V2L (Fig. 5c). Regarding the battery, in V2G higher current values were present, obtaining even a

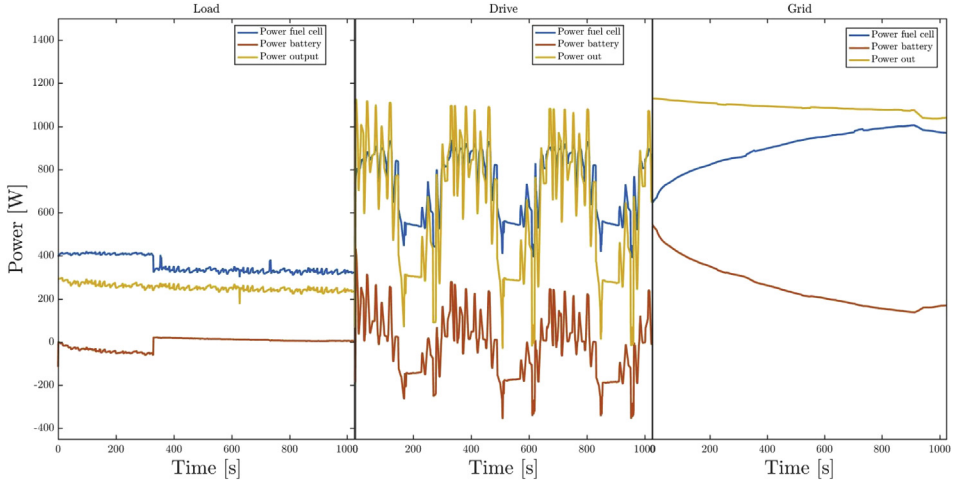

Fig. 4 – Power dynamics of the fuel cell (blue line), battery (red line) and power delivered to the electronic load (yellow) for the three scooter modes of operation; Vehicle-to-load (V2L), driving, and Vehicle-to-Grid (V2G). (For interpretation of the references to colour in this figure legend, the reader is referred to the Web version of this article.)

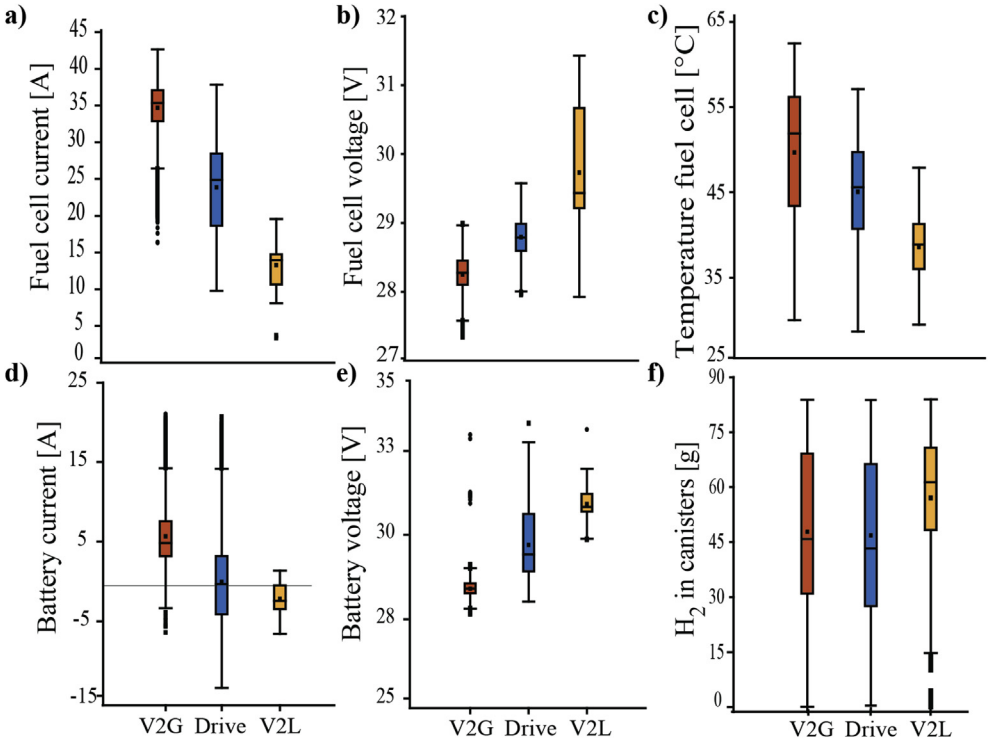

Fig. 5 – Data distributions under the V2G (red), drive (blue) and V2L (yellow) modes, corresponding to the following variables a) current, b) voltage and c) temperature of fuel cell, d) current and e) voltage of battery, and f) hydrogen content in the canisters. Central points within the boxplots represent the average value; boxes mark the 25th and 75th percentiles; horizontal lines outside the box, mark the values that extend 1.5 times the width of the box; points outside are outliers. (For interpretation of the references to colour in this figure legend, the reader is referred to the Web version of this article.)

negative average value for V2L (Fig. 5d). This is due to the dynamic operation of the hybrid system in V2L, in which the battery was only being charged by the fuel cell and no power was being delivered by the battery to the load. This led to higher average battery voltage values in V2L than in any of the other modes (Fig. 5e). Fig. 5f shows the boxplot for the hydrogen present in the canisters. It indicates that most of the tests in V2G and drive mode most where operated with full to empty tanks and that V2L mainly operated with full to intermediate tanks. Since less energy was demanded in V2L mode, less hydrogen was consumed during these tests and so the canisters where not depleted fully.

System efficiency

The only input of energy of the scooter is hydrogen via the canisters, as there is no electrical charging plug for the battery. Therefore, the efficiency of the hybrid system should consider the power from the fuel cell alone. The total system efficiency (η_{system}) was calculated using Eq. (1):

$$\eta_{system} = \frac{E_{out} - \Delta E_{battery}}{E_{H_2}} \quad (1)$$

where E_{out} is the electrical energy deliver to the load (either in drive, V2G or V2L mode), $\Delta E_{battery}$ is the difference in battery energy and E_{H_2} is the hydrogen energy consumption. $\Delta E_{battery}$ was calculated as the difference of energy discharged by the battery ($E_{battery,dis}$) and energy supplied from the fuel cell to charge it ($E_{battery,ch}$) during a full run, as shown in Eq. (2).

$$\Delta E_{battery} = E_{battery,dis} - E_{battery,ch} \quad (2)$$

The hydrogen energy consumption, E_{H_2}, was calculated as shown in Eq. (3),

$$E_{H_2} = \Delta m_{H_2} \times \mathrm{HHV} \quad (3)$$

where Δm_{H_2} is the difference of hydrogen mass at the start and end of the run, multiplied by the higher heating value of hydrogen. Thus the efficiency values informed in this study are based on HHV of hydrogen.

Using Eq. (1) yields the efficiencies depicted in Table 2. The overall system efficiency values shown here are average values obtained per mode.

As is shown in Table 2 and V2G resulted in the most efficient mode, followed by driving and V2L was the least efficient mode. Operating the system at almost maximum power, like

Table 2 – Average values for energy delivered, amount of hydrogen consumed and system total efficiency per mode.

	V2L	Drive	V2G
H_2 consumption (g)	16.8	13.8	7.6
Efficiency (%)	29	32	39

in V2G, is thus beneficial for using hydrogen efficiently: there is a relatively high amount of energy delivered by the scooter system in comparison with drive and V2L mode, relative to the amount of hydrogen energy fed in.

Ordination of modes according to the variables

Principal component analysis results show that it is possible to clearly identify the three modes of operation. Fig. 6 shows the PCA results in a biplot, where the individual runs are separated into three distinct groups. This type of plot is a combination of a scatter plot of the observations (each dot represents one of the 90 runs) and another scatter plot for the variables (represented by vector lines from the origin). The observations that are plotted in the same direction as a variable may have relatively high values for that variable and low value variables for those that are plotted in the opposite direction. The advantage of using PCA in this data set is that with only one plot we can see how all the variables are correlated and identify those that allow differentiating the modes of operation of the scooter.

The first principal component (PC1) separates fuel cell and battery voltage from the rest of the variables. In the biplot, this can be seen by focusing on the projection in the PC1 axis, which has negative values for these two variables. The rest of the variables have positive PC1 projection values. So, the greater variability between modes of operation of the scooter can be explained by these two variables. V2L (green dots) is more associated to high voltage values; V2G (blue dots) high (fuel cell and battery) current values, power output and temperature of the fuel cell. While driving (yellow dots) is an in between situation of these other two modes. Considering the second principal component axis, the most contributing variables are Battery Current and Fuel Cell Voltage, although the influence of these variables does not distinguish between modes. They do explain differences between runs and mainly in the V2L mode (green dots with more extent on the PC2 axis). These two axis explained 92.7% of the total variability among the 90 runs.

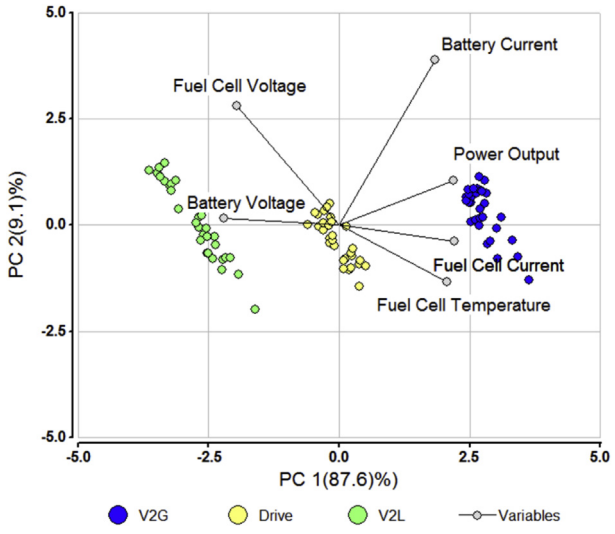

Fig. 6 – Visualization of the variability of runs in the space generated by the first two principal components of the Principal Component Analysis. Line vectors show the measured variables.

Voltage decline rate: performance comparison between modes

During usage over time of the fuel cell, its performance decreases because of aging/degradation mechanisms. This can be seen in the voltage-current profiles, where actual potential of the fuel cell decreases from its ideal potential due to irreversible losses in the system. These fuel cell irreversibility's contribute to the voltage drop of the system [38]. While there are different types of irreversible losses, in this work we assume all losses are result of Ohmic polarisation, since the fuel cell stack operates in an intermediate range of currents (see Fig. 7a, current values between 10 A and 40 A, whereas 5 A - 80 A is the operating range as stated by the manufacturer [39]). Ohmic losses occur due to flow of electrons at cathodes, flow of ions through electrolyte and interconnections between cells and bipolar plates. In this approximation, we can perform linear regression analysis (LRA) on the relationship between the voltage ($V_{Fuelcell}$) and current ($i_{fuelcell}$) of the fuel cell, as shown in Eq. (4):

$$V_{Fuelcell} = \beta_0 + \beta_1 * i_{fuelcell} \quad (4)$$

where $\beta_0$and $\beta_1$are the regression coefficients. Table 3 shows the results of the LRA partitioned by mode and in Fig. 7a the relationship between these two variables is plotted.

There is a clear decrease of the voltage with current increase in all three modes, as is expected when losses related to ohmic polarisation take place. The three modes operated in different stack output current ranges, therefore in the voltage decline analysis we focused on the slope of the regression as a parameter to compare between modes, not on the voltage values themselves. In the Ohmic approximation, β_1 can be understood as the equivalent resistance of the overall system. All coefficients values were statistically significant (p-value <0.0001). Comparing it between modes, we observe that the equivalent resistance in V2L mode was higher than in the other modes. Between Drive and V2G there was no difference observed. Resistance increase is a known effect as result of aging. The overall resistance was three times higher in V2L compared to the other modes. This indicates accelerated degradation in V2L mode compared to the other two modes. This higher loss of conductivity may result in faster degradation of the polymer membrane, the corrosion of the plates, dehydration of the membranes or corrosion of the catalyst support [40].

A commonly used parameter to measure degradation in fuel cells is the average cell voltage decline rate expressed in μV/h. Fig. 7b shows the average cell voltage values per mode plotted against accumulated experiment time. The average cell voltage was obtained by averaging all the cell voltage values of the FC stack for each of the 90 runs. The accumulated time corresponds to the total time implemented in the 90 runs. In all three modes, the slope of the resulting regression was negative, indicating degradation over time. Table 4 presents the results of this linear regression analysis.

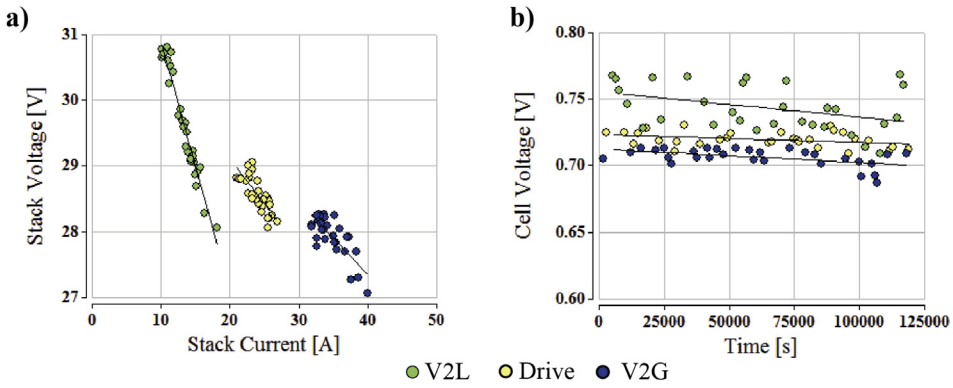

Fig. 7 – a) Fuel cell stack voltage relationship with current and b) average cell voltage vs. time.

All coefficients values, except β_1 for driving were statistically significant (p-value <0.05). This means that degradation has been observed in the experimental period and it is statistically significant in V2L and V2G mode, but in order to be significant in all the modes more repetitions would have to be done. During the 90 runs, the scooter was actively delivering power during 26 h in total, and it was operating approximately 8 h in stand-by. As fuel cells for transportation means are expected to have a lifetime of at least 5000 h [41], with actual measured values ranging around 2000 h in practice, 34 h performed in this work is relatively short.

β_1 is a rate of degradation parameter, as it states the change in voltage over a period of 1 s. Comparing it between modes V2L and V2G, higher degradation rate was present in V2L. This coincides with the previous PCA analysis. The degradation rates expressed in μV/h were 209 μV/h for driving mode, 356 μV/h for V2G and 648 μV/h for V2L. These values are in line with research performed on degradation analysis of fuel cell systems in road environment (as we have simulated here and as what the scooter was exposed before the experiments). For example, Li et al. reported an average cell voltage decline rate of 346 μV/h for fuel cell city buses [42]. Studies have found that the main factors leading to damage of PEMFC are frequent load changes, low power operation, and cold start-up [43–45]. As all the runs have been performed when the system was already warmed up, the latter is discarded as a cause in the performance decay observed. V2L was characterized by low power operation and frequent load change, causes explaining the higher degradation presented in this mode.

Table 3 – Results of the linear regression of fuel cell voltage vs. current presented per mode.

Mode	Coefficient	Estimate	S.E.	p-value
V2L	β_0 [V]	34.07	0.18	<0.0001
	β_1 [Ω]	−0.33	0.1	<0.0001
Drive	β_0 [V]	31.59	0.50	<0.0001
	β_1 [Ω]	−0.10	0.01	<0.0001
V2G	β_0 [V]	31.61	0.43	<0.0001
	β_1 [Ω]	−0.12	0.02	<0.0001

Table 4 – Results of the linear regression analysis of single cell voltage vs. time presented per mode.

Mode	Coefficient	Estimate	S.E.	p-value
V2L	β_0 [V]	0.75	0.01	<0.0001
	β_1 [V/s]	−1.8E-7	8.5E-8	0.0406
Drive	β_0 [V]	0.72	2.1E-3	<0.0001
	β_1 [V/s]	−5.7E-8	2.9E-8	0.0600
V2G	β_0 [V]	0.71	2.2E-3	<0.0001
	β_1 [V/s]	−9.9E-8	3.2E-8	0.0047

Conclusions

The combined use of a hydrogen electric scooter for driving and power generation was analysed in this study. The scooter was tested in three modes: to drive, to provide power to appliances (V2L) and to provide power to the grid (V2G). A two-stage statistical analysis method was implemented to understand the differences in the modes of operation and identify those variables leading to higher degradation of the fuel cell. First, Principal Component Analysis (PCA) led to the successful discrimination of the three modes of operation. The greater variability between modes could be explained by the fuel cell and battery voltage. Second, Linear Regression Analysis (LRA) was used to analyse the decay of fuel cell voltage with current and time, which allowed to determine the rate of degradation in the three different modes. V2L was identified as the mode that resulted in highest degradation of the fuel cell, due to lower operating power and higher operating voltage. V2G resulted in the most efficient mode using the fuel cell, since it operated at almost full load. Although, in the short period of test time degradation was observed in all modes, the statistical significance of the measurement of rate of degradation can be improved by increasing the testing time.

These results can be taken into account to design new specific energy management systems for V2L and V2G operation. As the actual energy system architecture of hybrid fuel cell/battery electric vehicles is designed for less degradation of the fuel cell in driving mode, we suggest that for V2L and V2G a different and new energy management system should be developed, parallel to the driving one. These should focus on high operating power, high current values and low operating voltages, to have less degradation effects on the fuel cell.

Acknowledgements

Funding from the European Union Horizon 2020 research and innovation programme is acknowledged under the ERA-Net Smart Grids plus grant agreement, No. 646039; from the Netherlands Organisation for Scientific Research (NWO); and from BMVIT/BMWFW, under the 'Energy der Zukunft' programme, which support the CESEPS project (www.ceseps.nl). Special thanks are given to Jaap van Raamt, Michel van den Brink and Martijn Karsten from DEMO section that helped us in the experimental set-up. The authors would like to acknowledge Athena Lin and APFCT for providing constant support and information.

REFERENCES

[1] International Energy Agency. Global energy & CO2 status report 2017. 2018.
[2] Mueller S, Frankl P, Sadamori K. Next generation wind and solar power. Int Energy Agency Books Online; 2016. https://doi.org/10.1787/9789264268715-en.
[3] Alanne K, Saari A. Distributed energy generation and sustainable development. Renew Sustain Energy Rev 2006;10:539–58. https://doi.org/10.1016/J.RSER.2004.11.004.
[4] Platt SM, Haddad I El, Pieber SM, Huang RJ, Zardini AA, Clairotte M, et al. Two-stroke scooters are a dominant source of air pollution in many cities. Nat Commun 2014;5:1–7. https://doi.org/10.1038/ncomms4749.
[5] Zhang X, Chan SH, Ho HK, Tan SC, Li M, Li G, et al. Towards a smart energy network: the roles of fuel/electrolysis cells and technological perspectives. Int J Hydrogen Energy 2015;40:6866–919. https://doi.org/10.1016/j.ijhydene.2015.03.133.
[6] Kolokotsa D. The role of smart grids in the building sector. Energy Build 2016;116:703–8. https://doi.org/10.1016/j.enbuild.2015.12.033.
[7] Pasaoglu G, Fiorello D, Martino A, Zani L, Zubaryeva A, Thiel C. Travel patterns and the potential use of electric cars - results from a direct survey in six European countries. Technol Forecast Soc Change 2014. https://doi.org/10.1016/j.techfore.2013.10.018.
[8] Barone G, Buonomano A, Calise F, Forzano C, Palombo A. Building to vehicle to building concept toward a novel zero energy paradigm : modelling and case studies. Renew Sustain Energy Rev 2019;101:625–48. https://doi.org/10.1016/j.rser.2018.11.003.
[9] Alanne K, Cao S. Zero-energy hydrogen economy (ZEH2E) for buildings and communities including personal mobility. Renew Sustain Energy Rev 2016:1–15. https://doi.org/10.1016/j.rser.2016.12.098.
[10] Doroudchi E, Alanne K, Okur Ö, Kyyrä J, Lehtonen M. Approaching net zero energy housing through integrated EV. Sustain Cities Soc 2018;38:534–42. https://doi.org/10.1016/j.scs.2018.01.042.
[11] Alirezaei M, Student PD, Noori M, Associate P, Tatari O. Getting to net zero energy building : investigating the role of vehicle to home technology. Energy Build 2016;130:465–76. https://doi.org/10.1016/j.enbuild.2016.08.044.
[12] Taehyung K, Vodyakho O, Yang J. Fuel cell hybrid electric scooter. Ind Appl Mag IEEEE 2011;17:25–31. https://doi.org/10.1109/MIAS.2010.939811.
[13] Kamakate (ICCT) F. Managing Motorcycles . 2009.
[14] van Wijk AJM. The green hydrogen economy in the Northern Netherlands. Noordelijke Innovation Board; 2017.
[15] Agency for Natural Resources and Energy. Compilation of the revised version of the strategic roadmap for hydrogen and fuel cells (METI). 2016. accessed, http://www.meti.go.jp/english/press/2016/0322_05.html. [Accessed 19 October 2018].
[16] Clean energy partnership n.d. accessed, https://cleanenergypartnership.de/en/home/. [Accessed 19 October 2018].
[17] H2.LIVE: Wasserstoff Tankstellen in Deutschland & Europa. 2018. accessed, https://h2.live/. [Accessed 19 October 2018].
[18] International Energy Agency. Technology roadmap. Hydrogen and Fuel Cells 2015. https://doi.org/10.1007/SpringerReference_7300.
[19] Schmidt O, Gambhir A, Staffell I, Hawkes A, Nelson J, Few S. Future cost and performance of water electrolysis: an expert elicitation study. Int J Hydrogen Energy 2017;42:30470–92. https://doi.org/10.1016/J.IJHYDENE.2017.10.045.
[20] Thounthong P, Chunkag V, Sethakul P, Davat B, Hinaje M. Comparative study of fuel-cell vehicle hybridization with battery or supercapacitor storage device. IEEE Trans Veh Technol 2009;58:3892–904. https://doi.org/10.1109/TVT.2009.2028571.
[21] Sripakagorn A, Limwuthigraijirat N. Experimental assessment of fuel cell/supercapacitor hybrid system for scooters. Int J Hydrogen Energy 2009;34:6036–44. https://doi.org/10.1016/j.ijhydene.2009.04.059.
[22] Lee C, Lin W. Stochastic self-optimizing power management for fuel cell hybrid scooters of different sized components. Int J Hydrogen Energy 2015;40:5197–209. https://doi.org/10.1016/j.ijhydene.2015.02.062.
[23] Hwang JJ. Sustainable transport strategy for promoting zero-emission electric scooters in Taiwan. Renew Sustain Energy Rev 2010;14:1390–9. https://doi.org/10.1016/j.rser.2010.01.014.
[24] Kempton W, Letendre S. Electric vehicles as a new power source for electric utilities. Transport Res Transport Environ 1997;2:157–75. doi:1361-9209/97.
[25] Kempton W, Tomic J, Letendre S, Brooks A, Lipman T. Vehicle-to-Grid power: battery, hybrid, and fuel cell vehicles as resources for distributed electric power in California. 2001.
[26] Cao S, Alanne K. The techno-economic analysis of a hybrid zero-emission building system integrated with a commercial-scale zero-emission hydrogen vehicle. Appl Energy 2018;211:639–61. https://doi.org/10.1016/j.apenergy.2017.11.079.
[27] Oldenbroek V, Verhoef LA, van Wijk AJM. Fuel cell electric vehicle as a power plant: fully renewable integrated transport and energy system design and analysis for smart city areas. Int J Hydrogen Energy 2017;42:8166–96. https://doi.org/10.1016/j.ijhydene.2017.01.155.
[28] Oldenbroek V, Hamoen V, Alva S, Robledo C, Verhoef LA, van Wijk AJM. Fuel cell electric vehicle-to-grid: experimental feasibility and operational performance as balancing power plant. Fuel Cells 2018. https://doi.org/10.1002/fuce.201700192 Fuel.
[29] Robledo CB, Oldenbroek V, Abbruzzese F, van Wijk AJM. Integrating a hydrogen fuel cell electric vehicle with vehicle-to-grid technology, photovoltaic power and a residential building. Appl Energy 2018;215:615–29. https://doi.org/10.1016/j.apenergy.2018.02.038.
[30] Hwang JJ. Review on development and demonstration of hydrogen fuel cell scooters. Renew Sustain Energy Rev 2012;16:3802–15. https://doi.org/10.1016/j.rser.2012.03.036.
[31] Hu X, Song K, Niu W, Zhang T. Powertrain system durability in proton exchange membrane fuel cell electric vehicles: a

review. SAE Tech Pap 2018:1–12. https://doi.org/10.4271/2018-01-1303. 2018–April.
[32] Kim T, Vodyakho O, Yang J. Fuel cell hybrid electric scooter. Development of zero-emission vehicles. IEEE Ind Appl Mag 2011:25–31.
[33] Tzeng GH, Chen JJ. Developing a Taipei motorcycle driving cycle for emissions and fuel economy. Transport Res Transport Environ 1998. https://doi.org/10.1016/S1361-9209(97)00008-4.
[34] Lin B. Conceptual design and modeling of a fuel cell scooter for urban Asia. J Power Sources 2000. https://doi.org/10.1016/S0378-7753(99)00480-2.
[35] Robledo JI, Sánchez HJ, Leani JJ, Pérez CA. Exploratory methodology for retrieving oxidation state information from X-ray resonant Raman scattering spectrometry. Anal Chem 2015;87:3639–45. https://doi.org/10.1021/ac5035677.
[36] Placca L, Kouta R, Candusso D, Blachot J-F, Charon W. Analysis of PEM fuel cell experimental data using principal component analysis and multi linear regression. Int J Hydrogen Energy 2010;35:4582–91. https://doi.org/10.1016/j.ijhydene.2010.02.076.
[37] Di Rienzo JA, Casanoves F, Balzarini MG, Gonzalez L, Tablada M, Robledo CW. InfoStat 2014. Grupo InfoStat.
[38] Kaur G. Solid oxide fuel cell components: interfacial compatibility of SOFC glass seals. 2015. https://doi.org/10.1007/978-3-319-25598-9.
[39] APFCT. IV polarisation curve supplied by scooter manufacturer. 2019.
[40] Fowler MW, Mann RF, Amphlett JC, Peppley BA, Roberge PR. Incorporation of voltage degradation into a generalised steady state electrochemical model for a PEM fuel cell. J Power Sources 2002;106:274–83. https://doi.org/10.1016/S0378-7753(01)01029-1.
[41] DOE. US Department of Energy Technical Targets for Polymer Electrolyte Membrane Fuel Cell Components n.d. accessed, https://www.energy.gov/eere/fuelcells/doe-technical-targets-polymer-electrolyte-membrane-fuel-cell-components. [Accessed 15 October 2018].
[42] Li J, Hu Z, Xu L, Ouyang M, Fang C, Hu J, et al. Fuel cell system degradation analysis of a Chinese plug-in hybrid fuel cell city bus. Int J Hydrogen Energy 2016;41:15295–310. https://doi.org/10.1016/j.ijhydene.2016.06.136.
[43] Schmittinger W, Vahidi A. A review of the main parameters influencing long-term performance and durability of PEM fuel cells. J Power Sources 2008;180:1–14. https://doi.org/10.1016/j.jpowsour.2008.01.070.
[44] Wahdame B, Candusso D, François X, Harel F, Péra MC, Hissel D, et al. Comparison between two PEM fuel cell durability tests performed at constant current and under solicitations linked to transport mission profile. Int J Hydrogen Energy 2007;32:4523–36. https://doi.org/10.1016/j.ijhydene.2007.03.013.
[45] Luo Y, Guo Q, Du Q, Yin Y, Jiao K. Analysis of cold start processes in proton exchange membrane fuel cell stacks. J Power Sources 2013;224:99–114. https://doi.org/10.1016/j.jpowsour.2012.09.089.